

# Characterizing spatiotemporal patterns in three-state lattice models

Matti Peltomäki<sup>1</sup>, Martin Rost<sup>2</sup> and Mikko Alava<sup>1</sup>

<sup>1</sup> Department of Applied Physics, Helsinki University of Technology, P.O. Box 1100, 02015 HUT, Espoo, Finland

<sup>2</sup> Bereich Theoretische Biologie, IZMB, Universität Bonn, 53115 Bonn, Germany

E-mail: matti.peltomaki@tkk.fi

**Abstract.** A two-species spatially extended system of hosts and parasitoids is studied. There are two distinct kinds of coexistence; one with populations distributed homogeneously in space and another one with spatiotemporal patterns. In the latter case, there are noise-sustained oscillations in the population densities, whereas in the former one the densities are essentially constants in time with small fluctuations. We introduce several metrics to characterize the patterns and onset thereof. We also build a consistent sequence of corrections to the mean-field equations using *a posteriori* knowledge from simulations. These corrections both lead to better description of the dynamics and connect the patterns to it. The analysis is readily applicable to realistic systems, which we demonstrate by an example using an empirical metapopulation landscape.

**Keywords:** population dynamics (theory), stochastic particle dynamics (theory), pattern formation (theory), cellular automata

PACS numbers: 87.23.Cc 02.50.Ey 82.20.-w 87.18.Hf

## 1. Introduction

Pattern formation has gained a lot of interest in both the physical [1, 2, 3, 4, 5, 6, 7, 8, 9, 10, 11, 12, 13, 14, 15, 16] and the ecological [17, 18, 19, 20, 21, 22] literature. Patterns may either emerge from the dynamics itself or reflect the structure of the underlying landscape. Since the mechanism of pattern formation plays a crucial role, for instance, in ecological systems when one is concerned about extinctions of species [17, 23, 24], it is of fundamental interest to be able to pin down the essential mechanism.

The classical model of two-species systems, such as predator–prey or host–parasitoid systems, is the Lotka–Volterra (LV) model [25]. It assumes fully stirred, or panmictic, species. However, introducing explicit space typically leads to correlated structures where the assumption breaks down [17]. The correlations manifest themselves in a wide variety of forms. The most common ones are spray-like or flame-like in spatial dimensions [1, 19, 20, 22], ripple-like in space–time [20], and spiral-like [16, 18, 21, 24]. Similar patterning has also been observed in several related models in statistical physics [3, 5, 10, 8, 12, 15], in chemical surface catalysis [2, 4, 6, 7, 11, 9], in calcium signaling in cells [26, 27, 28], and in the infamous complex Ginzburg–Landau equation (CGLE) [29], for instance.

In ecological and chemical systems, the correlations typically weaken the interactions, since species tend to be aggregated within themselves. They also provide the prey (host) a spatial refuge since around the prey (host) there are less predators (parasitoids). This is called the spatial rescue effect [17]. Altogether, spatial inhomogeneity can stabilize the dynamics and strengthen population coexistence [17, 20, 30] even via several different mechanisms [23]. Spatial two-population dynamics can also lead to counter-intuitive effects in which increasing the host (prey in prey–predator systems) spreading rate actually leads to smaller host population sizes [31]. Understanding spatiotemporal dynamics in highly fragmented landscapes [32] is of even greater difficulty.

There are also myriads of empirical observations of the patterning in ecological systems. Among the most intriguing examples are field voles in Northern Britain with evidence of traveling waves [33], mussel beds in the Wadden Sea in the Netherlands with regular spatial patterns [34] together with voles [35] and lemmings [36] in Northern Europe. Recently, similar studies have also been performed in experimental laboratory conditions [37].

In this contribution, we study a numerical model of spatially extended two-population, or three-state, dynamics. We formulate the model in terms of hosts and parasitoids but in the scope of this work, these are interchangeable with prey and predator, respectively. It is defined on a regular square lattice, and the spreading of the species occurs in a distance-dependent way according to the corresponding incidence functions (see below). There are two regimes of coexistence: the species can be either distributed homogeneously in space, or build up spatial correlations or patterns (see Fig. 1).

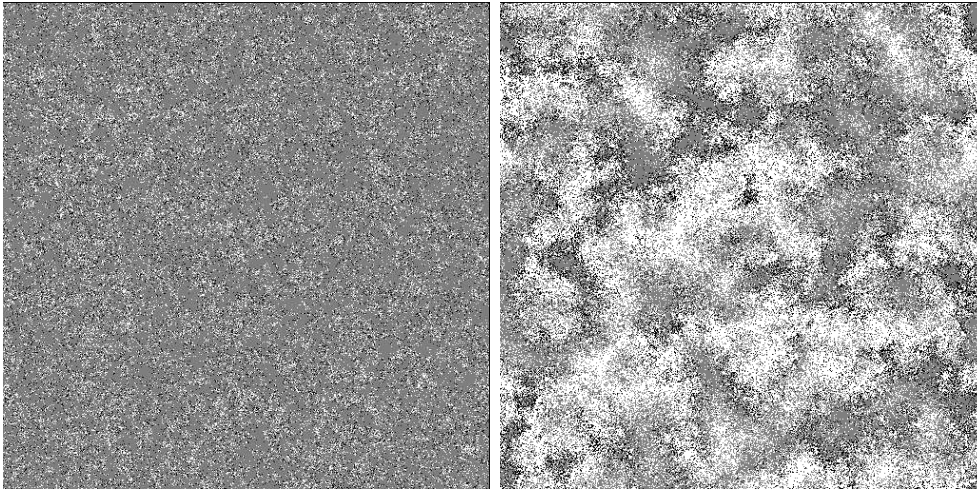


**Figure 1.** Two snapshots of the system with coexistence. Left: disordered homogeneous structure for parameters  $w_h = 3.0$ ,  $w_p = 1.5$ ,  $\lambda_h = 0.63$ ,  $\lambda_p = 1.3$ , and  $\delta = 0.9$ . Right: a patterned state; parameters are as in the non-patterned one except for  $\lambda_p = 2.5$ . Sites with  $e$  are white, gray stands for  $h$ , and  $p$  is shown in black.

We study the system from two points of view. The first one concentrates on the patterns, which we first coarse-grain into areas dominated by one of the species or empty space. They give rise to vortices as the corner points of three different areas, and domain walls as the boundary lines between them. We introduce several quantities describing the geometry and dynamics of these objects. They include the instantaneous velocities of the vortices, their number and lifetime, the average length of the domain walls and the shape of the dominance areas close to the vortices. All these quantities support the division of the parameter space into two kinds of coexistence.

The second point of view is that of the global dynamics of the system. Here, we extend on our previous results [38] in which we have shown that for large enough systems there are no non-linearities and in the spatially correlated coexistence regime, the global dynamics is governed by noise-sustained oscillations not conforming to the traditional limit cycles. See Fig. 2 for examples of the corresponding time series. We show that the linearization coefficients differ from what one gets from the complete mixing, or mean-field, assumption, that this is caused by the dependence of the effective spreading parameters on the instantaneous global population densities, and that this dependence is vastly different in the two different coexistence regimes. We also link the dynamics together with the patterns by showing that the former one can be understood as an infinite stream of aperiodically occurring spontaneous synchronizations.

Both the tools for the patterns classification and the analysis of the dynamics are not restricted to the particular case studied here. Foremost, they are not restricted to two species (or three states) or two spatial dimensions. In addition, their domain of applicability does not lie in ecology only; the voter models of statistical physics [3, 5, 10, 8, 12, 15] and certain surface catalysis reactions [2, 4, 6, 7, 11, 9] lead to similar

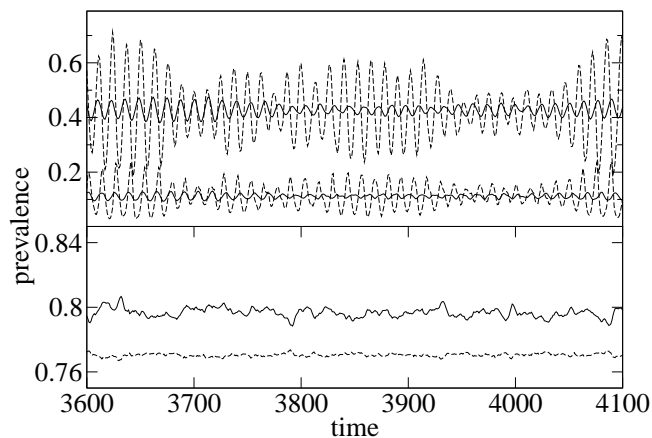


**Figure 2.** Upper panel: the population densities in the patterned state for a system of size  $L = 512$  (solid lines), and a subsystem of size  $L = 64$  (dashed lines) of a similar one. The upper curves correspond to hosts and the lower ones to parasitoids. The parameters are as in Fig. 1. Lower panel: the population densities in the homogeneous state for the hosts (solid line) and parasitoids (dashed line) for a system of size  $L = 512$ . The latter line has been shifted upwards for clarity. The parameters are as in the upper panel except for  $\lambda_p = 1.3$ .

patterning, and sometimes similar dynamics, as well, and the machinery discussed here provides means to characterize and classify the patterns also in these areas.

This paper is organized as follows. In Sec. II the model is defined in detail together with the coarse-graining procedure, vortices, domain walls and quantities derived from them. The section also discusses the program to correct the MF equations. In Secs. III and IV the results regarding patterns and dynamics, respectively, are presented and discussed. Sec. V contains an example application of the analysis, and Sec. VI discusses the results both from the physical and the ecological point of view and makes connections to earlier and contemporary literature. Finally, Sec. VII wraps up the paper and concludes.

## 2. Model

### 2.1. Definition

The model describes annual host–parasitoid dynamics on a regular two-dimensional square lattice  $\Lambda$ . It is inspired by Ref. [39] but has a wider interaction range as typical in metapopulation dynamics [32]. At a given time, a lattice site can be empty (state  $e$ ), populated by a host either without ( $h$ ) or with ( $p$ ) parasitoids. The dynamics allows for a cycle of transitions,  $e \rightarrow h \rightarrow p \rightarrow e \rightarrow \dots$ . This is a simplification that neglects the decay of the hosts on their own, and in turn emphasizes the role of the parasitoids. In particular, spontaneous deaths of non-parasitized hosts are assumed to be rare enough to be considered nonexistent. Even though this means that hosts live forever if parasitoids are absent, the restriction is not serious. In coexistence it reduces to assuming faster

typical extinction times for the parasitoids than for the hosts. An equivalent description of the model is as a variant of the susceptible-infected-recovered (SIR) model [40] with longer spreading lengths and rebirth. Here, the infected state corresponds to hosts, the recovered one to parasitoids, and the rebirth to the spontaneous death of the parasitoids.

The transition probabilities between the states are functions of the *connectivities* which in turn depend on the local populations and are thus directly related to the number of immigrants arriving at a lattice site. For a given configuration, the connectivity of species  $h$  or  $p$  on lattice site  $x$  at time  $t$  is

$$I_{h|p}(\mathbf{x}, t) = \sum_{\mathbf{x}'} k_{h|p}(|\mathbf{x} - \mathbf{x}'|) \chi_{h|p}(\mathbf{x}', t) \quad (1)$$

where  $\chi_{h|p}(\mathbf{x}, t)$  is the characteristic function, i.e. = 1 if the state of  $\mathbf{x}$  at time  $t$  is  $h$  or  $p$ , respectively, and = 0 else. The kernel has an exponential decay with a characteristic scale  $w_{h|p}$

$$k_{h|p}(|\mathbf{x} - \mathbf{x}'|) \propto \exp\left(-\frac{|\mathbf{x} - \mathbf{x}'|}{w_{h|p}}\right), \quad (2)$$

and is normalized such that its integral over the whole plane equals one. In time step  $t \rightarrow t + 1$ , the transition  $e \rightarrow h$  takes place with probability  $\lambda_h I_h$  and transition  $h \rightarrow p$  with probability  $\lambda_p I_p$ . The parasitoids die out (the transition  $p \rightarrow e$ ) with probability  $\alpha$  irrespective of the surroundings. Parallel updates are used. There is an absorbing state with the lattice completely filled with hosts without any parasitoids, together with long-lived reactive coexistence states.

There are numerous assumptions in the model from the ecological point of view. The first and foremost are the long-range interactions. In realistic cases, they are particularly important for the stability of the system since they contribute to immigration and survival also in remote habitat patches. In a regular lattice, their role is not as emphasized. The assumption, however, is fairly weak, since the dispersal takes place according to an exponentially decaying kernel, i.e. there is a typical short interaction length. Furthermore, the connectivity (1) is defined such that parasitized hosts do not contribute to the host connectivity. Naturally, this is not completely true in empirical systems, since unparasitized hosts can be found also in parasitized habitat patches and these are fully capable of contributing to the spreading of the hosts. All these assumptions are minor ones and they do not hinder one from being able to tackle the relevant and interesting properties of the model system.

In the MF approximation, the behavior of the system can be calculated as follows. The rate equations for the population densities are

$$\begin{aligned} h_{t+1} &= h_t + \kappa(1 - h_t - p_t)h_t - \mu p_t h_t \\ p_{t+1} &= p_t - \delta p_t + \mu p_t h_t, \end{aligned} \quad (3)$$

where the coupling constants  $\kappa$  and  $\mu$  are just the total transition rates obtained under constant densities. There are three fixed points: the coexistence

$$\bar{h} = \frac{\delta}{\mu} \quad \text{and} \quad \bar{p} = \frac{\kappa(\mu - \delta)}{\mu(\kappa + \mu)} \quad (4)$$

if  $\mu \equiv \mu(\bar{h}, \bar{p}) > \delta$ , the extinction of parasitoids

$$\bar{h} = 1 \quad \text{and} \quad \bar{p} = 0 \quad (5)$$

otherwise, and the extinction of both species

$$\bar{h} = 0 \quad \text{and} \quad \bar{p} = 0 \quad (6)$$

which is achieved if the hosts die out before the parasitoids do. The coexistence fixed point can be either stable or unstable depending on the parameters. The unstable case corresponds to a limit cycle. Below, we compare these elementary observations to the behavior of the spatially extended system. Since the MF approximation is merely a rough one, there is no particular reason to expect one-to-one correspondence.

## 2.2. Characterizing patterns

To characterize the patterns, consider a spatially smoothed continuous field of population densities [38]

$$\rho_{h|p,w}(\mathbf{x}, t) \equiv \sum_{\mathbf{x}'} k_w(|\mathbf{x} - \mathbf{x}'|) \chi_{h|p}(\mathbf{x}', t), \quad (7)$$

where the smoothing kernel  $k_w(\mathbf{x})$  is a two-dimensional Gaussian such that  $\sum_{\mathbf{x}} k_w(\mathbf{x}) = 1$ ,  $\sum_{\mathbf{x}} \mathbf{x} k_w(\mathbf{x}) = \mathbf{0}$ , and  $\sum_{\mathbf{x}} \mathbf{x}^2 k_w(\mathbf{x}) = w^2$ . Here the variance  $w$  is called the smoothing width, and the summation runs over all lattice sites. At each site  $\mathbf{x}$ , the smoothed densities  $\rho_{h|p,w}(\mathbf{x}, t)$  oscillate around the temporally and spatially averaged densities

$$\bar{h} = \frac{1}{N} \lim_{T \rightarrow \infty} \frac{1}{T} \sum_{t=1}^T \sum_{\mathbf{x}} \chi_h(\mathbf{x}, t) \quad (8)$$

and

$$\bar{p} = \frac{1}{N} \lim_{T \rightarrow \infty} \frac{1}{T} \sum_{t=1}^T \sum_{\mathbf{x}} \chi_p(\mathbf{x}, t). \quad (9)$$

We use these to divide the two-dimensional phase space spanned by the densities into three sectors, defined in the caption of Fig. 3. They are then used to divide the system into *prevalence domains* so that site  $\mathbf{x}$  at time  $t$  is defined to belong to a domain according to the region of the phase space containing the smoothed densities at location  $\mathbf{x}$ , i.e.  $(\rho_h(\mathbf{x}, t), \rho_p(\mathbf{x}, t))$  in Eq. (7). The regions coarse-grain on a scale somewhat larger than the typical interaction lengths. They are not sensitive to changes in the smoothing width  $w$  given that it is larger than the interaction lengths and smaller than the system size  $L$ .

The domains readily give rise to more sophisticated quantities. To start, define the vortices as the corner points of the three different types of domains. These are associated with a positive or negative unit “charge” since one can encounter the three domains in two different orders by traversing a circle around it in a given direction (say, counter-clockwise). Similar structures with three kinds of domains rotating around their corner points without any coarse-graining have been identified earlier in statistical physics in the context of the three-state voter model [5], the extended three-state voter

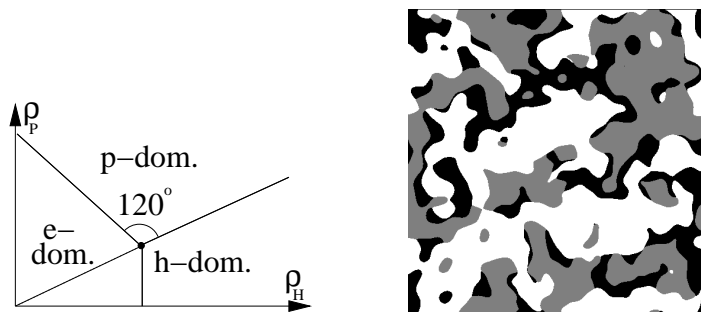


**Figure 3.** (a) The division of the phase space into three sectors associated with the three states,  $e$ ,  $h$  and  $p$ . For given average densities  $\bar{h}$  and  $\bar{p}$ , the first quadrant of the  $(\rho_h, \rho_p)$ -plane is divided into three regions by three lines. That separating  $h$ - and  $p$ -dominated regions starts from the average  $(\bar{h}, \bar{p})$  (the black dot), goes towards increasing  $\rho_h$  and  $\rho_p$  and is such that its continuation (the dotted line) passes through the origin. The other two lines form 120-degree angles with the first one and each other. (b) The computed dominance regions of the configuration shown in Fig. 1.

model and the three-state Potts model [13], and combinations thereof [10, 15]. Also a four-state model with game-theoretical inspirations [14] shows similar vortices. In three dimensions, the vortices generalize to strings [1]. Further, the domain walls are defined as the boundary lines between two domains of different types. There are three kinds of walls, according to the possible three pairs of domain types they separate, and exactly one wall of any given type emanates from a given vortex. The vortices and domain walls provide simple means to describe the population patterns, as we demonstrate below.

To derive quantities that follow the evolution of the vortices and domain walls in time, it is necessary to be able to reliably track their motion. To this end, we have implemented the following procedure. Let the  $A_-$  and  $A_+$  be the sets of vortices with negative and positive sign, respectively, at time  $t$ . Denote by  $B_-$  and  $B_+$  the same after one discrete time step, i.e. at time  $t + 1$ . An interpretation for the movements of the vortices, including creation and annihilation or pairs, is a simple pairing of the sets  $X = A_- \cup B_+$  and  $Y = A_+ \cup B_-$ . If an element  $(x, y)$  of this pairing consists of vortices in  $A_-$  and  $B_-$  ( $A_+$  and  $B_+$ ) a negatively (positively) charged vortex is interpreted to have moved but not annihilated. If the element consists of vortices in  $A_-$  and  $A_+$ , the two vortices are considered to have annihilated with each other, and, finally, if the element is a pair of vortices from  $B_-$  and  $B_+$ , the vortices are considered to be newly created vortices at time step  $t + 1$  that did not exist at time  $t$ .

There is an enormous number of such pairings, and physically motivated means of selecting one are needed. To this end, define a fully connected weighted bipartite graph  $G = (X, Y, E, w)$ , where the vortex sets  $X$  and  $Y$  are the vertices, the edge set their Cartesian product  $E = X \times Y$ , and the weight function  $w$  assigns each edge  $(x, y)$  a weight equal to the Euclidean distance between vortices  $x$  and  $y$ . We use the so-called Hungarian method from graph theory to obtain the pairing of the sets  $X$  and  $Y$  that has the minimum total weight. This pairing is then used to interpret the motion,

annihilation, and creation of the vortices as described above. The Hungarian method itself is a well-known exact optimization algorithm for the bipartite pairing problem based on graph flows. It is fairly complex but it runs in cubic time with respect to the number of elements in the sets to be paired. Detailed explanations of it can be found in the literature [41, 42].

Building on the tracking procedure for the vortices, it is simple to outline a similar procedure for the domain walls. We consider a given wall observed at time  $t$  to be the same wall as another one at time  $t + 1$  if and only if it is of the same type (separates the same two domain types) and if both its endpoint vortices are identified as the same according to the method above. A necessary condition for this is that the vortices have not been annihilated.

After implementing these identification procedures, the vortices and walls can be used to derive a practically unlimited number of quantities that, in a way or another, describe the dynamics or the statics of the patterns. Here, we have used several, selecting the ones considered most suitable. These include the jump length of the vortices, i.e. distance traveled by a vortex in unit time, the number and lifetime of vortices, the geometry of the domains in the immediate vicinity of the vortices described by the widths of the sectors the domains form around them, and the lengths of the domain walls themselves. See Fig. 4 for a schematic illustration of some of these quantities.

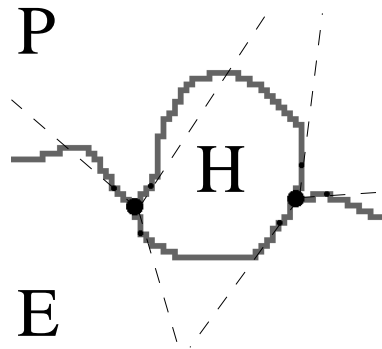


**Figure 4.** An illustration of the vortices, the domain walls, and the tangents of them describing the geometry of the walls near the vortices. The background is a magnified portion of Fig. 3 with all three domains colored white and marked with capital letters, and the boundaries marked gray. The locations of the vortices are shown with thick black circles. The smaller black circles show lattice sites on the wall that are at the distance of  $w_t = 5$  lattice units from the vortices, and the dashed lines drawn via the vortices and these points are the domain wall tangents.

Upon applying these metrics, attention must be paid to the fact that random fluctuations around the average densities also create vortices and domain walls. This is an unfortunate side effect of the definitions that must not be neglected but has to be taken into account. This is especially important in the case of the domain wall lengths, in which the fluctuations give rise to a nonzero background level, and it is the deviations of the wall length statistics from this background – not from zero – that



signals the onset of patterns. Here, we take the background into account by creating random configurations of the system by assigning each lattice site a state of  $e$ ,  $h$ , or  $p$  randomly using the spatiotemporally averaged densities  $\bar{h}$  and  $\bar{p}$  from a simulation as the occurrence probabilities of the respective states. The background vortex and wall length levels are then obtained by computing the same metrics for these random configurations.

### 2.3. Effective mean-field dynamics

The MF equations (3) discussed in the Introduction assume full mixing both within a single species and between two species. In spatially extended systems, such as the one studied here, the assumptions fail almost invariably. There are several known ways to incorporate spatial effects. These include, for example, pair approximations [43, 44, 45, 46, 47], rescaling the coordination number of the lattice [48], and others [49]. Here, our approach is to use input from numerical simulations to introduce corrections of different order to the MF equations. These corrections are such that there is no need to specify a functional form for the interactions before the analysis.

The zeroth-order correction is to consider the change in the effective values of the spreading rate parameters introduced by the spatial effects. This is done by running the simulations for different values of the parameters, obtaining the average population densities as a function of them, and subsequently using the inverse of Eqs. (4) to arrive at those effective values of the MF parameters that lead to the densities observed in the simulations. However, common experience suggests that this kind of rescaling of the parameters is an utterly implausible explanation for the spatial effects. Instead, higher order schemes have to be used.

The first-order correction builds on the zeroth-order one. Now, in addition, the effective parameters are considered functions of the instantaneous population densities  $h_t$  and  $p_t$ . For  $\lambda_\alpha I_\alpha(\mathbf{x}, t)$  small, they equal the spreading probabilities, and thus dynamics can be written as [38]

$$h_{t+1} = h_t + \sum_{\mathbf{x} \in \Lambda} \left[ \lambda_h k_h(\mathbf{x}) C_{eh}(\mathbf{x}, t) - \lambda_p k_p(\mathbf{x}) C_{hp}(\mathbf{x}, t) \right] \quad (10)$$

and

$$p_{t+1} = (1 - \delta)p_t + \lambda_p \sum_{\mathbf{x} \in \Lambda} k_p(\mathbf{x}) C_{hp}(\mathbf{x}, t), \quad (11)$$

where the influence of the connectivities on the prevalence dynamics is expressed by the correlation functions

$$C_{\alpha\beta}(\mathbf{x}, t) = \frac{1}{|\Lambda|} \sum_{\mathbf{x}' \in \Lambda} \chi_\alpha(\mathbf{x}', t) \chi_\beta(\mathbf{x} + \mathbf{x}', t). \quad (12)$$

An approximation of these equations can be written as (cf. Eqs. (3))

$$\begin{aligned} h_{t+1} &= h_t + \kappa(h_t, p_t) (1 - h_t - p_t) h_t - \mu(h_t, p_t) p_t h_t \\ p_{t+1} &= p_t - \delta p_t + \mu(h_t, p_t) p_t h_t. \end{aligned} \quad (13)$$

This is an approximation of the usual MF form with the interaction parameters  $\kappa(h, p)$  and  $\mu(h, p)$  generalized to be arbitrary functions of the instantaneous densities. The full form of them seems to be in general not obtainable analytically. In general, they can be nonlinear, and in particular they do not have to conform to the standard LV model nor to any ad-hoc approximations discussed in the literature, for example turning the coordination number of the lattice into two effective coordination numbers that serve as phenomenological parameters separately for the hosts and the parasitoids [48]. To arrive at the first-order correction, perform a series expansion of Eqs. (11) around the fixed point  $(\bar{h}, \bar{p})$  and introduce auxiliary variables  $\eta_t$  and  $\pi_t$  such that  $h_t = \bar{h} + \eta_t$  and  $p_t = \bar{p} + \pi_t$ . Doing this, we arrive to linear order at

$$\begin{pmatrix} \eta_{t+1} \\ \pi_{t+1} \end{pmatrix} = \begin{pmatrix} a_{h,h} & a_{h,p} \\ a_{p,h} & a_{p,p} \end{pmatrix} \begin{pmatrix} \eta_t \\ \pi_t \end{pmatrix} \quad (14)$$

with the matrix elements

$$\begin{aligned} a_{h,h} &= 1 + \kappa - 2\kappa\bar{h} - (\kappa + \mu)\bar{p} + \partial_h \kappa \bar{h}(1 - \bar{h} - \bar{p}) - \partial_h \mu \bar{h}\bar{p} \\ a_{h,p} &= -(\kappa + \mu)\bar{h} - \partial_p \kappa \bar{h}(1 - \bar{h} - \bar{p}) - \partial_p \mu \bar{h}\bar{p} \\ a_{p,h} &= \mu\bar{p} + \partial_h \mu \bar{h}\bar{p} \\ a_{p,p} &= 1 - \delta + \mu\bar{h} + \partial_p \mu \bar{h}\bar{p}, \end{aligned} \quad (15)$$

in which  $\mu$ ,  $\kappa$ , their derivatives, and the population densities are evaluated at the fixed point  $(\bar{h}, \bar{p})$ .

If the four derivatives are set to zero in Eq. (15), Eqs. (14) and (15) fall back to the mean-field approximation, and the matrix in Eq. (14) is directly the linearization matrix usable for the standard stability analysis. On the other hand, if the derivatives are nonzero, the mean-field analysis is not valid anymore. This situation can be interpreted as instantaneous densities affecting the spreading rates.

As we have demonstrated earlier [38] and will elaborate on below, the linear form of Eqs. (14) and (15) can be readily fitted to temporal data from simulations of the spatially extended model, and numerical values for the matrix elements can be easily obtained. This allows one to solve for the four derivatives,  $\kappa$  and  $\mu$  with respect to  $h$  and  $p$ , and subsequently arrive at the first order correction to the MF equations. Note that this computation reveals the domain of applicability of the mean-field treatment by either yielding vanishing derivatives (applicable) or non-vanishing ones (not applicable). In principle, the procedure could be continued *ad infinitum* to higher derivatives leading to higher-order corrections. These calculations are omitted here, however, since the linear treatment turns out to be enough to demonstrate and discuss the effect of the corrections. Note that the program outlined here is by no means restricted to the present model, but it can be applied to virtually any other one with a similar structure. In particular, it is not restricted to two-species (or three-state) models, two spatial dimensions and not even to discrete time, since continuous-time results can always be retrospectively discretized by sampling snapshots, nor discrete space. Promising candidates for such an application include those in Refs. [3, 5, 10, 8, 12, 15, 50, 51, 52, 53], for example.

### 3. Patterns

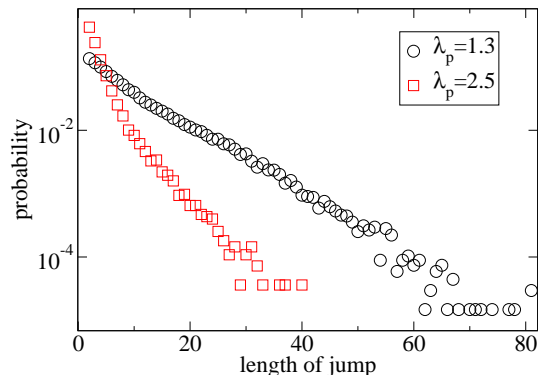


**Figure 5.** Distribution of the jump length of the vortices, i.e. the distance traveled by a vortex in unit time, in both the non-patterned ( $\lambda_p = 1.3$ ) and the patterned ( $\lambda_p = 2.5$ ) case. Other parameters are as in Fig. 1. The average jump lengths are approximately 3.6 and 9.2 lattice units for  $\lambda_p = 2.5$  and  $\lambda_p = 1.3$ , respectively.

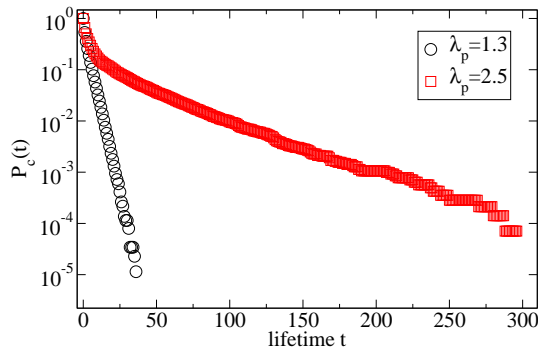


**Figure 6.** Cumulative distribution of the vortex lifetime according to the tracking algorithm in non-patterned and patterned cases. See the caption of Fig. 5 for the values of the parameters. The average lifetimes are approximately 2.9 and 8.7 discrete time units for  $\lambda_p = 1.3$  and  $\lambda_p = 2.5$ , respectively.

The vortices and the domain walls can be located and followed through time as described in Section 2.2. In general, considering quantities derived from these leads to an observation of two distinct kinds of coexistence regimes. There is one with formation of chaotic moving fronts, patterns, and another one without them. All computations discussed in detail below support the division.

First, we consider the jump length of the vortices, i.e. the distance a given vortex moves in unit time. A histogram of these is plotted in Fig. 5 for the values of the parasitoid spreading rate parameter  $\lambda_p$  corresponding to the patterned and the non-patterned cases. Both distributions are exponential, but the patterned case has a clearly smaller average jump length than the non-patterned one. Similarly, we plot the lifetime distributions of the vortices in the same  $\lambda_p$  two cases in Fig. 6. Now, the difference between

them is even bigger; in the patterned case the vortices live typically ten times as long as in the non-patterned case. Therefore, with patterns the vortices are more stable than without them both with respect to movements and annihilation. Were the typical vortex jump lengths considered in units of the typical pattern size (for example, the average domain wall length discussed below), the difference between the two cases would be even more pronounced.

In a more detailed inspection, the vortex lifetime distribution in the patterned case ( $\lambda_p = 2.5$ ) in Fig. 6 is composed of two parts; for short lifetimes the distribution follows that of the non-patterned case, and for long lifetimes, there is a broad tail. A direct consideration of the definition of a vortex reveals the cause. Namely, vortices can, roughly speaking, originate in two different ways. They can be either signs of a “real” inhomogeneous structure such as seen in Fig. 1, or merely random fluctuations around the average population densities. The former leads to the wide tail, whereas the latter shows up as the short-lifetime part of the distribution.

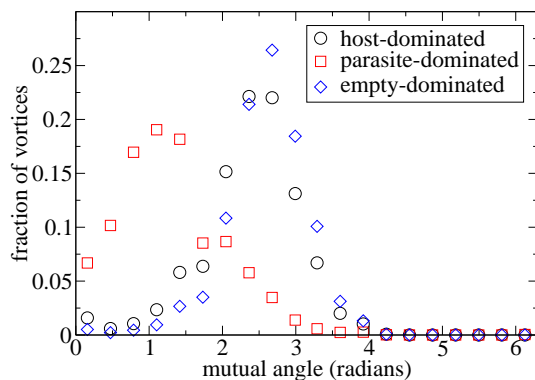


**Figure 7.** The distributions of the angles between the tangent directions of the three domain walls at a vortex (see Fig. 4). The angles are multiplied by the vortex charge so that for each vortex the three domains are passed in the same direction. The data is from the patterned state, and parameters are as in Fig. 1.

Next, we turn to the geometry of the dominance regions in the vicinity of the vortices. We compute the angles between the tangent lines of the three walls (see Fig. 4) and plot the distributions in the patterned case in Fig. 7. The parasite-dominated sectors appear to be rather narrow (typically 60 degrees) in comparison to the host- and empty-dominated ones, whose typical spread equals approximately 160 degrees. This is somewhat balanced by the larger variance of the width of the parasite-dominated sectors. In any case, these observations conform to those one can make by studying the appearance of Fig. 3 in the vicinity of the vortices by bare eye.

The ratio of the measured domain wall length and its counterpart in random configurations is plotted in Fig. 8 as a function of the two spreading rate parameters,  $\lambda_h$  and  $\lambda_p$ . The parameter space is clearly divided into two regions with a continuous crossover in between by this quantity. In one of these parts, the ratio equals approximately one (corresponding to homogeneous population densities), whereas in the

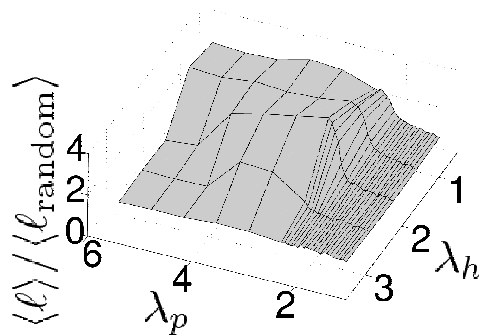


**Figure 8.** The ratio of the measured average domain wall length to its counterpart in random configurations as a function of the parasitoid and host spreading rate parameters  $\lambda_p$  and  $\lambda_h$ . The ratio is approximately one in the uniformly distributed case and increases to approximately three in the patterned case. In all cases, the distribution of the domain wall lengths decays exponentially (not shown). Other parameters are as in Fig. 1.

other, the ratio clearly differs from one (corresponding to pattern formation). In other words, in cases where the system does not exhibit patterns visible to human eye, the domain wall length statistics also coincides with that in a spatially homogeneous case, whereas with patterns there is a significant difference. Note, however, that the numerical value of the ratio bears no meaning by itself, since it can be tuned to almost any value by altering the smoothing kernel (in particular the smoothing width  $w$ ) in the coarse-graining procedure. Nevertheless, for any usable value of  $w$ , the ratio clearly deviates from one and therefore is a usable metric of the patterning. The transition between the cases is continuous everywhere on the transition line. We have also considered similar statistics for the average vortex jump length and the average vortex lifetimes, recovering a continuous crossover in each case.

Given all these results on the vortices, the domain walls, and their dynamics, there remains the question of how much of them can be explained by considering the vortices as identical random walkers with random signs in a plane. To study this point in detail, we have performed numerical experiments consisting of a set of simulated random walks for a given value of the simulation parameters as follows. For each walk, draw its duration  $N_{rw}$  randomly using the measured vortex lifetime distribution. Let each walk start at the origin and perform  $N_{rw}$  random steps. For each step, draw the jump length from the corresponding measured jump length distribution and choose the direction in two dimensions randomly from a uniform distribution. Record the average total length of the walks for each case of interest, i.e. for different simulation parameters (and consequently different measured distributions).

In the non-patterned and patterned cases, we get average total walk lengths of 20 and 9 lattice units, respectively, in the random walk experiment. In the non-patterned case, this roughly corresponds to half of the average domain wall length which, in

turn, approximately equals the average inter-domain distance. Therefore, the picture of vortices as merely uncorrelated random walkers cannot be ignored. On the other hand, there is more than an order of magnitude of difference between the average domain wall and random walk lengths. This rules out any explanation of the dynamics of the system that is based on the random walk picture only.

Finally, we take a look at the behavior of the number of vortices as a function of time. A relevant benchmark for comparison is the complex Ginzburg-Landau equation (CGLE) which has been studied extensively (for a good review, see [29]). Both in the usual deterministic version of the equation [54], and in a version with added noise [55], the number of pairs of vortices  $n(t)$  has been observed to be a Markov process with  $n(t)$ -dependent creation and annihilation rates. An essential feature of such processes is the lack of memory of any kind. We have partially repeated the analysis of Refs. [54, 55] in the present case. Average creation and annihilation rates as a function of  $n(t)$  can be measured once a sufficient number of realizations of the process have been simulated. Doing this, we arrive at a description similar to Eqs. (3) and (4) of [55]. In other words, the creation rate is a constant and the annihilation  $\Xi_-(n)$  rate assumes the form

$$\Xi_-(n) = An^2 + Bn \quad (16)$$

where  $A$  and  $B$  are constants. In this respect the number of vortices behaves here in the same way as in the CGLE. However, a detailed look reveals again an important difference. In the present case, the number of vortices as a function of time contains an oscillatory component clearly visible both in the time series itself and its Fourier power spectrum. This cannot be explained by a one-dimensional memoryless dynamical system, and therefore the vortex number statistics lies outside the realm of applicability of the analysis of Refs. [54, 55].

Instead, to recreate the vortex number process, short-term memory has to be incorporated in a way or another. One way to do this is to consider a two-dimensional process where the role of the second variable is played by the first discrete time derivative of the vortex number  $n$ . This leads to a description similar to Eqs. (14) and (15) for the vortex number and its derivative. On the other hand, the same process can be formulated in terms of the second time derivative or a temporal delay. In any case, one-dimensional processes such as Eq. (16) do not suffice.

## 4. Dynamics

### 4.1. Effective mean-field

To gain insight on the dynamics of the system, and to produce the effective low-order corrections to the MF equations, we have used Poincaré maps [56] reconstructed from simulations. Here, the dynamical (scalar) variables of the system at time  $t + 1$  are considered to be functions of the same at time  $t$ . This mapping is then numerically computed from measurements of the dynamical variables from the simulations of the model. In particular, in the case of two dynamical variables, a graphical representation

of the Poincaré maps boils down to two three-dimensional scatter plots. We draw them for two different system sizes in the patterned case and for comparison in the non-patterned one in Fig. 9. Immediate conclusions can be made. There is indeed a clear functional dependence of the densities on their previously assumed values. In other words, the dynamics can be described by using the densities themselves only; as a dynamical system the present one is two-dimensional. This would not have been obvious given the  $2L^2$  discrete degrees of freedom in the spatially extended system.

We have also verified this conclusion using attractor reconstruction [57]. There, a simulated time series is studied using a variable number  $N_d$  of degrees of freedom, which are the time series itself as such, and with suitable delays  $\tau$ ,  $2\tau$ ,  $3\tau$ , and so on. Here, we have used a quarter of the time of a period as the time delay  $\tau$ . With two dynamical variables,  $h(t)$  and  $h(t - \tau)$  we find that there is a unique mapping (up to noise) from their values at time  $t$  to their values at time  $t + 1$ . Such mapping does not exist if only one dynamical variable is used, and these findings hold also when  $p(t)$  (and the corresponding delayed variable) is used instead of  $h(t)$ . Therefore, attractor reconstruction duplicates the conclusion from above that the system has two degrees of freedom as a macroscopic dynamical system.

Based on the numerical observations, the dynamics can be cast as an analogous pair of equations to (3) but with different functional forms. Even further, the plots are clearly linear in both variables for a large system size (here  $L = 512$ , Figs. 9a and 9b), whereas for smaller system sizes ( $L = 64$ , Figs. 9c and 9d) there are deviations from the linear form. The point clouds are stretched towards the absorbing state of the system with extinct parasitoids. The necessary system size for the onset of linearity can be crudely estimated by visual inspection. It reveals the rough approximation  $L_{\text{lin}} \approx 120$ , slightly larger than the corresponding average domain wall length (see Sec. 3). Thus, the linearity is obeyed, if the system is large enough to accommodate several domains.

To arrive at an effective MF iteration based on the Poincaré plots valid for large systems, we perform least-squares fits to them and arrive at Eq. (14) with numerically determined coefficients  $a_{\sigma,\sigma'}$ . This picture takes space implicitly into account since the interaction parameters (or the matrix elements) are automatically suitably adapted to the form and parametrization of the manifolds. In addition to this deterministic description, the system exhibits noise whose magnitude – both perpendicular and tangential to the manifolds – is proportional to the square root of the system size. Also, after the pure noise component and the deterministic picture above have been removed, one is left with a residue that comes from the approximation made in the linearization. However, for large system sizes this residue is small when compared to the linear deterministic component and the noise. The numerically fitted coefficients  $a_{\sigma,\sigma'}$  come into play below during the discussion of the effective parameters and sustained oscillations.

The predictions of the MF theory of Eqs. (3) for the host and parasitoids densities compared with those obtained from simulations are shown in Fig. 10. The host density  $\rho_h$  does not depend on the host spreading rate parameter  $\lambda_h$  according to the MF theory

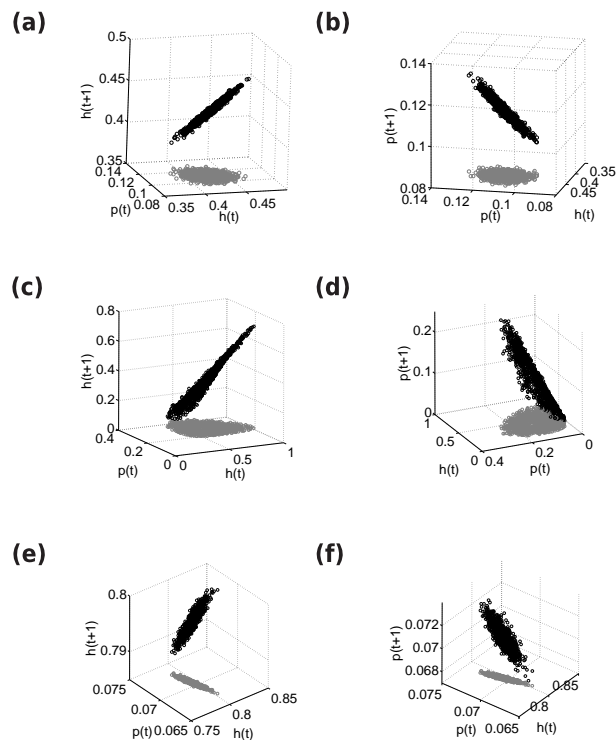


**Figure 9.** The Poincaré maps illustrating the dynamics of the system. (a), (b):  $h_{t+1}$  and  $p_{t+1}$  as a function of  $h_t$  and  $p_t$  for a system in the patterned state (parameters as in Fig. 1a) with size  $L \times L = 512 \times 512$ . (c), (d): The same for a system of size  $64 \times 64$ . (e), (f): As in (a) and (b) but for a system in the homogeneous state, i.e. with  $\lambda_p = 1.3$ . The simulations have been run for 3000 time steps and data was gathered for the last 1000.

and as is seen from the figure, this is almost the case also in simulations. On the other hand, the parasitoid density  $\rho_p$  depends strongly on both spreading rate parameters  $\lambda_h$  and  $\lambda_p$  both in the MF theory and in the simulations. Altogether, Fig. 10 shows that the MF approximation works surprisingly well in predicting the species densities. Note however, that these comparisons are only for the average densities and do not constitute evidence of the validity of the MF theory in other respects, such as the stability of the fixed point or the nature of oscillations, if any.

In order to arrive at equations that can also predict these more complicated issues, we proceed in two phases. The first one – here called the zeroth-order correction – is to ask which values of the parameters have to be inserted into the MF equations so that they give the same population densities as the simulations. In other words, the question is what are the effective MF spreading rate parameters as a function of the simulational ones. To this end, we have run simulations for a wide range of parameters and computed the effective host and parasitoid spreading rates  $\kappa_{\text{eff}}$  and  $\mu_{\text{eff}}$  by using the inverse of Eq. (4). The results are plotted in Fig. 11. The conclusions are evident. The dependence is strongly nonlinear, as was expected, and the immediate observation is therefore that the effective parameters cannot be obtained from the simulational ones



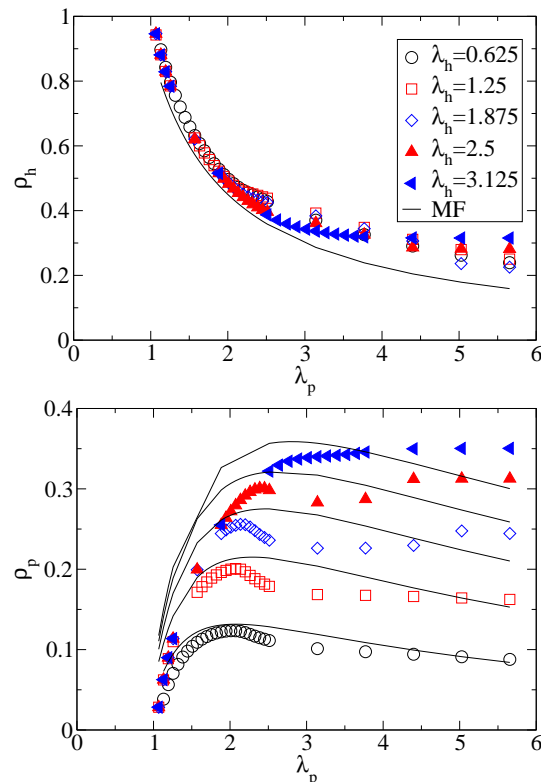


**Figure 10.** Prevalences as functions of the spreading rate parameters  $\lambda_{h|p}$ , together with the MF predictions. The prediction for  $\rho_h$  does not depend on  $\lambda_h$ , whereas the for  $\rho_p$  predictions for  $\lambda_h = 0.625, 1.25, 1.875, 2.5$  and  $3.125$  from bottom to top are shown. The color code is the same in both panels.

by any simple rescaling. Furthermore, the division between the patterned and non-patterned regions of the parameter space is clearly visible in Fig. 11. It shows up as a ridge in  $\kappa_{\text{eff}}$  and as a bend in  $\mu_{\text{eff}}$ .

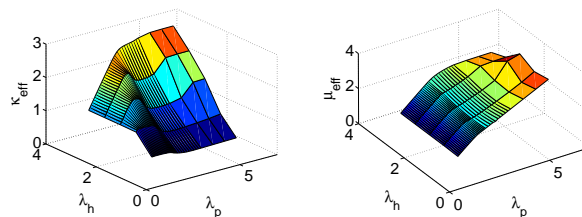


**Figure 11.** Effective values of the parameters  $\kappa$  (left) and  $\mu$  (right) as a function of the input parameters  $\lambda_h$  and  $\lambda_p$ .

In addition to what has been discussed above, the effective parameters do depend on the population densities within single realizations with fixed parameters. Here, we call this dependence the first-order correction, and it is the one that causes changes in the effective iteration equations with respect to Eqs. (3). Indeed, given the described dependence,  $\kappa$  and  $\mu$  in Eqs. (3) are functions of  $h_t$  and  $p_t$  as opposed to constants.

To compute the first-order correction, linearize Eqs. (3) around the reactive fixed point assuming that  $\kappa$  and  $\mu$  are functions of the population densities. One arrives at Eq. (14), in which there are four matrix elements that are linear in the four unknown first derivatives of  $\kappa$  and  $\mu$  with respect to  $h_t$  and  $p_t$ . The matrix elements are then set to equal those obtained from linear fits to the Poincaré plots, i.e. the  $a_{\sigma,\sigma'}$  in Eq. (14), and the unknown derivatives are solved for.

The results are shown in Fig. 12, in which for each considered value of the parameters  $\lambda_h$  and  $\lambda_p$  the derivatives are drawn as an arrow depicting the magnitude and direction of the gradient of  $\kappa$  and  $\mu$  with respect to  $h_t$  and  $p_t$ . The auxiliary coordinate system on the bottom left corner fixes the orientation of the gradients. The behavior of  $\mu_{\text{eff}}$  is especially interesting. In the non-patterned case the derivatives practically vanish. This means that the rate parameters  $\kappa$  and  $\mu$  are effectively constants and that the MF theory is a rather good approximation. This, in turn, means that the populations are well-mixed. On the other hand, the derivative of  $\mu_{\text{eff}}$  with respect to  $p_t$  clearly deviates from zero and assumes negative values in the patterned case. This is a direct sign of the insufficiency of the MF theory in this parameter regime. The correlations that for a larger number of parasitoids, makes them aggregated within themselves and thus decreases the “free boundary” available for spreading constitute one contributing factor to this insufficiency.

We have also checked the consistency of the computations above by solving for the effective  $\kappa$  and  $\mu$  from the MF iteration equations (3) separately for each time step, and considered these as a function of the population densities. The results are in an excellent numerical agreement with those above. In principle, the fits of the functional form in Eq. (14) could be extended to any order, and used together with the higher-order counterparts of the analysis of the derivatives of  $\kappa$  and  $\mu$  above to extract the derivatives up to any order.

#### 4.2. Oscillations

With patterns the population densities oscillate with an amplitude that fluctuates in time (Fig. 13). Without patterns, the densities fluctuate randomly around a stable fixed point. The angular frequency of the oscillation can be measured by performing three-dimensional linear fits to the Poincaré maps (Fig. 9) and extracting the imaginary part of the eigenvalues of the resulting matrix  $a_{\sigma,\sigma'}$  in Eq. (14). The MF prediction for the frequency is computed similarly. These are compared in Fig. 14. The frequencies from the MF theory and the simulations have roughly the same numerical values, but the agreement is far from perfect.

Instead of the oscillations themselves, the most characteristic property of the population densities is the fluctuation of the amplitude. The typical amplitude depends both on the parameters and the system size (see Fig. 2). Decreasing the system size increases it but keeps the qualitative behavior and the population densities intact. We have previously given an explanation for the amplitude fluctuations [38] which we here

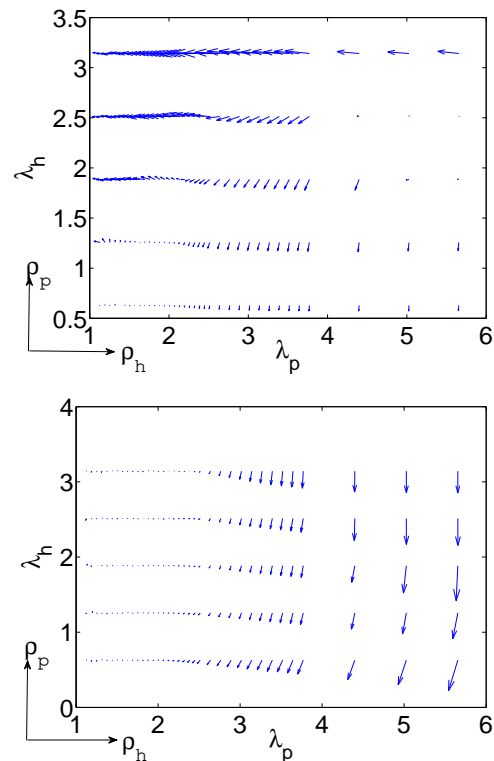


**Figure 12.** The first-order dependence of the effective parameters on the population densities  $\rho_h$  and  $\rho_p$ . At each point, the arrow depicts the derivative of  $\kappa_{\text{eff}}$  (above) and  $\mu_{\text{eff}}$  (below) according to the auxiliary coordinate system drawn on bottom left. The same points of the parameter space are sampled as in Fig. 11.

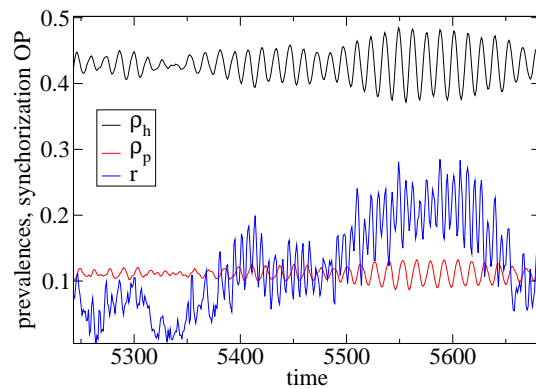


**Figure 13.** Time series of host and parasite prevalences, and the synchronization order parameter  $r$  (Eq. (18)). The parameters are as in Fig. 1. The amplitudes of the oscillations correlate strongly with each other and with the values of  $r$ . See Fig. 2 for the dependence of the amplitudes on the system size.

briefly rephrase. Namely, both with and without patterns, the fixed point of the effective (deterministic) iteration given by the fits to the Poincaré maps is stable. As such, there should be no oscillations in either case. However, the eigenvalues of the iteration matrix

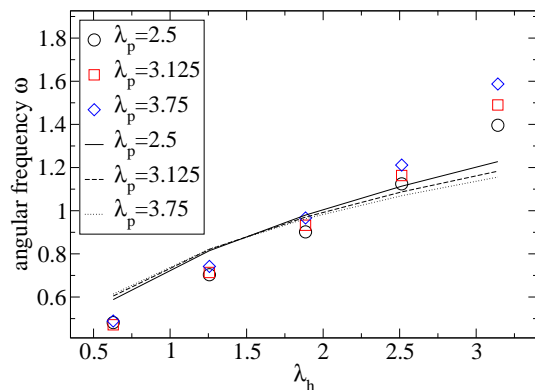


**Figure 14.** The angular frequency of the sustained oscillations as a function of the host spreading rate parameter  $\lambda_h$  for several values of  $\lambda_p$ . The frequency is measured as the polar angle of the eigenvalues of the linear fit of the simulation data to Eq. (14). The measurements are done for a system of size  $L \times L = 512 \times 512$  which is large enough for the linear fits to work well. Other parameters are as in Fig. 1. The solid, dashed, and dotted lines show the frequency predicted by MF theory, i.e. linearization of Eq. (3) and numerical solution of the resulting eigensystem.

are a complex-conjugated pair in both cases, and the transients towards the fixed point are oscillatory. Such transients give naturally rise to two independent time scales, one for the oscillation (time of a period) and another one for the decay. Denoting the eigenvalue pair as  $\rho e^{i\phi}$ , the ratio of the time scales is

$$\nu = \frac{\tau_{\text{decay}}}{\tau_{\text{osc}}} = \frac{\phi}{\log \rho}. \quad (17)$$

Inspecting this numerically reveals small values without patterns and large values with them. Therefore, in the latter case any fluctuations away from the fixed point lead to slow oscillatory convergence towards the fixed point which is repeatedly disrupted by stochasticity giving rise to a perpetual decay – noise-sustained oscillations.

Note that when approaching the stability limit from below,  $\rho$  approaches one, and the ratio  $\nu$  diverges towards positive infinity. With  $\rho > 1$ , the ratio reassumes finite values, now with a negative sign, but does not anymore carry the same physical meaning as below the limit.

The time scale ratio  $\nu$  both measured from simulations and predicted by the MF equations and the excess domain wall length (the difference between the average domain wall length and its value in random configurations) are plotted in Fig. 15 as a function of the parasitoid spreading rate parameter  $\lambda_p$ . The behavior of  $\nu$  is drastically different between simulations and theory. In the latter case, the ratio diverges at around  $\lambda_p = 1.9$  and assumes negative values at higher  $\lambda_p$ . In other words, the system undergoes a bifurcation from a stable fixed point to an unstable one characterized by a limit cycle. On the other hand, the simulated time scale ratio  $\nu$  peaks around almost the same point, but does not in fact diverge, signaling that there is no limit cycle involved. To see the connection between the temporal and spatial properties of the system, note that the

dependence of the average domain wall length and the time scale ratio on the parasitoid spreading rate parameter  $\lambda_p$  is similar for  $\lambda_p < 2.2$ . This can be interpreted as direct evidence that the pattern formation and the deviations of the dynamics from the MF description are closely intertwined. Also the behavior of the time scale ratio and the excess line length is qualitatively similar for  $\lambda_p > 2.2$  since both are constants in this regime. This is comparable to the coupled discrete oscillators of Wood and co-workers [52, 53], where a related system has a second-order synchronization transition in the MF theory and in higher dimensions but not in two.

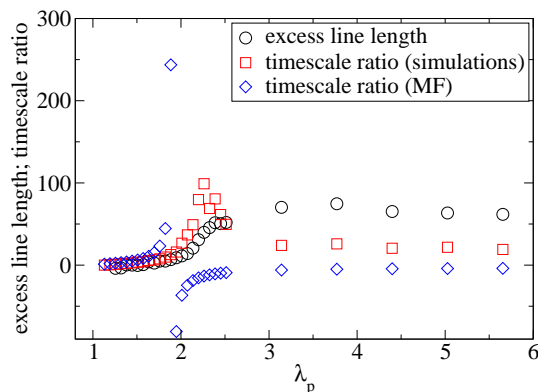


**Figure 15.** The timescale ratio of Eq. (17) in both the simulations and the MF theory plotted together with the difference between the average domain wall length in the actual simulation and in random configurations. All other parameters except for  $\lambda_p$  are as in Fig. 1.

There is also another straightforward spatial interpretation of the amplitude fluctuations. Consider the system divided into small boxes whose width is clearly smaller than the typical width of the coarse-grained patterns, but which at the same time are large enough so that local self-averaging occurs inside each box. Now a local phase  $\phi_i$  for each box  $i$  can be defined as the phase angle of the population densities inside the box with respect to the average densities (see Fig. 3). Given these, the degree of synchronization between the boxes can be defined as is customary in the context of the Kuramoto model for coupled oscillators [58]

$$r = \frac{1}{N} \left| \sum_j e^{i\phi_j} \right|, \quad (18)$$

where the summation runs over all  $N$  boxes.

In this computation, we have used the box size  $l \times l = 64 \times 64$  in accordance with the criteria above, and computed the synchronization order parameter  $r$  for each time step. This is plotted in Fig. 13 together with the host and parasitoid densities in the same simulation run. The amplitude of the density oscillations correlates strongly with  $r$ . This is to be interpreted such that the system spontaneously synchronizes over at least intermediate length scales at random intervals. As a feature of secondary importance, the synchronization order parameter  $r$  oscillates with a time of a period half of that

of the population densities, which is also seen in the Fourier power spectrum of  $r$  (not shown).

### 4.3. Phase diagram

Given the fact that the noise-sustained oscillations can be interpreted in terms of spontaneous synchronization, it is an interesting question whether it is macroscopic in character or “merely” a finite-size effect. To address this issue, we have computed the temporal average of the synchronization order parameter  $r$  (18) for different system sizes  $L$  both in the patterned and non-patterned cases. The results are shown in Fig. 16. In all cases, the scaling  $r \sim L^{-1}$  is found (similarly to [52, 53]). Thus, we conclude that the system does not show long-range order and thus does not completely synchronize at macroscopic scales.

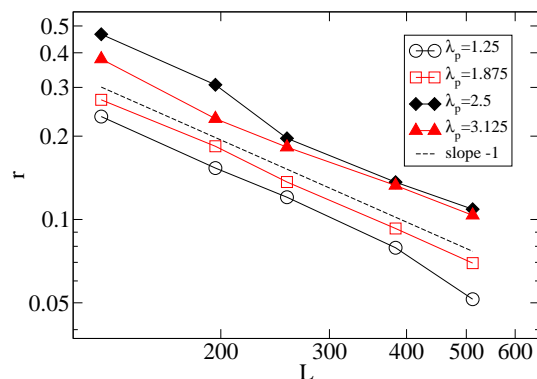


**Figure 16.** The synchronization order parameter  $r$  of Eq. (18) as a function of system size  $L$  for several values of  $\lambda_p$ . In each case, the scaling  $r \sim L^{-1}$  is found, demonstrating the lack of long-range order in the system.

In spite of this, the phase diagram remains interesting. In addition to the extinction transition of the parasitoids, the coexistence phase can be split into three. There are the non-patterned and the patterned regions, and since the crossover between them is not sharp a “gray area” between them. We have built the phase diagram in the  $(\lambda_h, \lambda_p)$ -plane by defining the boundary between the non-patterned case and the gray area to be the line at which the timescale ratio  $\nu$  of Eq. (17) equals 1.0, and that of the gray area and the patterned phase where the ratio equals 4.0. Albeit arbitrary, these definitions seem fit since upon looking at the population densities as a function of time and figures such as Fig. 1, the patterns and the oscillations are clearly not there if the ratio is below one, and, on the other hand, if it exceeds 4, both are clearly observed. Note that the timescale ratio assumes values as high as 100 (see Fig. 15). The qualitative features of the phase diagrams are not sensitive to altering the limiting values of  $\nu$ .

The phase diagrams are shown in Fig. 17 for two choices of the spreading widths  $w_h$  and  $w_p$ . It is seen that for any value of  $\lambda_h$  the four phases (parasitoid extinction, homogeneous coexistence, the gray area, and patterned coexistence) follow each other

in this order if the parasite spreading rate parameter  $\lambda_p$  is increased. This feature does not depend on the particular values of the spreading widths, or even their mutual order. The phase structure bears some resemblance to related earlier models [44, 46, 47] in that oscillatory and non-oscillatory regions and a boundary between them is recovered. See Sec. 6 for a detailed discussion and comparison. Fig. 17c also shows the vortex density, i.e. number of vortices per lattice site, as a function of  $\lambda_p$ . One sees that the number of vortices decreases rapidly while going from the nonoscillatory region via the gray area to the oscillatory regime.

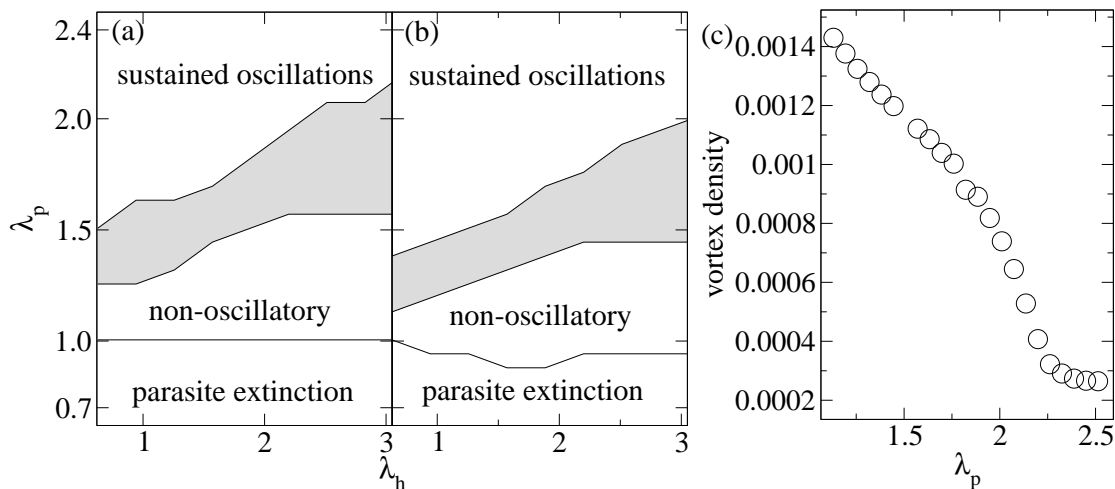


**Figure 17.** Phase diagrams with varying  $\lambda_h$  and  $\lambda_p$ , for different spreading ranges. (a)  $w_h = 3$  and  $w_p = 1.5$ , (b) switched  $w_h = 1.5$  and  $w_p = 3$ . In both cases four “phases” are found, parasite extinction, coexistence without oscillations, coexistence with oscillations, and a gray area between the two, which is due to the fact there is not, in fact, a sharp transition between the oscillatory and non-oscillatory regimes, but a continuous cross-over. The upper and lower bounds of the gray area are defined as the lines where the timescale ratio of Eq. (17) equals 1 and 4, respectively. The system size is  $L \times L = 512 \times 512$ . (c) The vortex density as a function of the parasitoid spreading rate parameter  $\lambda_p$  for the case of panel (a) with  $\lambda_h = 0.63$  and the smoothing width  $\sigma = 8$ .

Finally, we note that even if the system does not in general synchronize macroscopically, such synchronization can be artificially achieved by making the system small with respect to the spreading widths. This can originate in either making the system really small, or keeping the size fixed and increasing the spreading widths. In these cases, the MF theory probably works better than in what has been studied here. This, however, lies outside the scope of interest since extremely small system sizes or very large spreading lengths are needed.

## 5. A realistic example

To give a concrete example of how to apply the methods introduced here, we illustrate the role of coherent dynamics in biological systems by resorting to a well-known

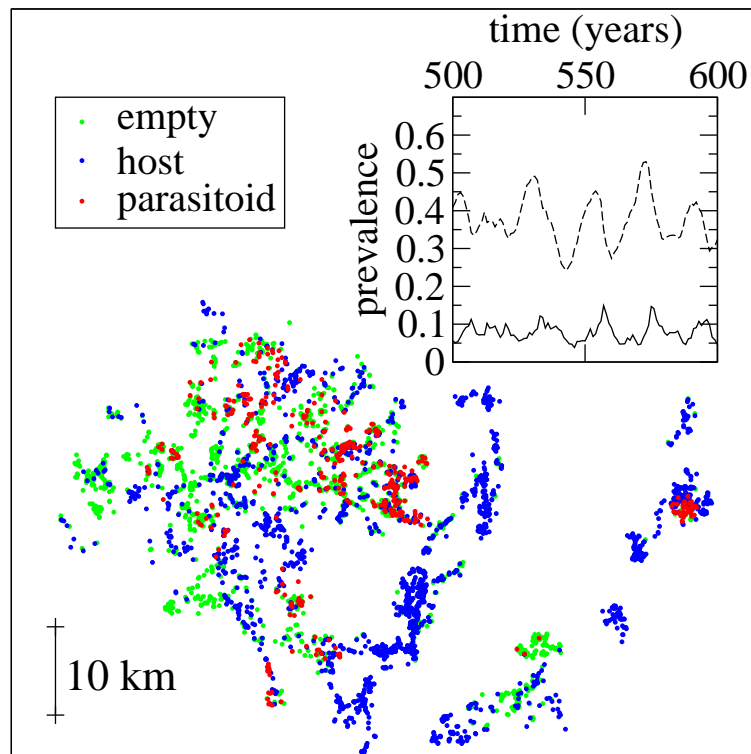
metapopulation system, investigated at length by the Metapopulation Research Group at University of Helsinki, Finland [32, 59, 60, 61, 62]. The species in question are the Glanville fritillary butterfly *Melitaea cinxia* and its specialist parasitoid wasp *Cotesia melitaeorum* on the network of habitats on the Åland islands in the Baltic Sea (60° N, 20° E) between Finland and Sweden. Here we use the known patch geography as the “lattice”. The two populations follow a variant of the model used above, with the differences that the contribution of each patch to the connectivities is multiplied by its area, and that in addition to the connectivity-driven spreading a small amount of uniformly random reproduction is used. These differences are biologically motivated. Intuitively, the immigration pressure from a given patch increases with the local population, which itself is positively coupled to the amount of locally available suitable habitat, the patch size. The random spreading mimics occasional long-range dispersal, and its effect is to prevent extinction on remote subnetworks, which are naturally present at the outskirts of the sparse archipelago. Also, open boundaries are used. This does not restrict the validity of the analysis for two reasons. First, the equations (14) are an observation made *from* the simulations, and by plotting the Poincaré maps as in Fig. 9, one sees that the equations hold both for open and periodic boundaries. Second, the equations (15) are obtained from Eqs. (13) by straightforward differentiation, and Eqs. (11), in turn, are a rough approximation equally valid in either case.

Fig. 18 shows a snapshot of the system, and the inset contains the respective time series; see the caption for the parameters. The question is now, do we find evidence of oscillations and/or patterns here? A similar analysis of the dynamics, from Eq. (14) is readily carried out, revealing the eigenvalues  $\lambda_{\pm} \approx 0.84 \pm 0.17i$  for the parameters used in Fig. 18. These imply, in accordance with the appearance of the time series, that the system contains patterns and exhibits oscillations coming from the combination of an unstable fixed point with oscillatory transients and demographic stochasticity. The patterning is clearly visible in Fig. 18. It can be analyzed using the smoothed densities by considering the sum in the expression for them, Eq. (7), as a summation over the patches, and using the position-dependent smoothed densities assuming average population densities at each patch as the triple point in the phase space (see Fig. 3a). The rest of the analysis can then be carried out as explained in Section 2.2. Doing this, one finds a domain structure analogous to that on the regular lattice with the average domain wall length  $\langle \ell \rangle / \langle \ell_{\text{random}} \rangle \approx 1.8$ .

These observations are of interest for a couple of reasons. First, the Åland landscape is rather heterogeneous, and at a closer inspection [63] appears to consist of a variety of densely connected subsystems, which are weakly coupled to each other. Due to the differences in the landscape with respect to a regular lattice, it is not clear, a priori, that the whole system has similar pattern-included noise-sustained oscillations as the version defined on a regular lattice. Instead, the expectation for a single densely connected subsystem is to be closer to the mean-field limit [45] obeyed by a fully connected (essentially non-spatial) system, and since the number of such dense subsystems is relatively small, the expectation is the same for the full system. However, noise-



sustained oscillations are observed, and the Åland system works as an example of the applicability of the analysis presented here to more realistic cases, than regular lattices. This is emphasized by the fact that also the dynamics of the model contains differences with respect to the lattice one, in addition to the spatial structure. In any case, the eigenvalues of the effective iterative map (Eq. (14)) provides information about the stability properties and the level of patterning in the system.



**Figure 18.** Main figure: a snapshot of the simulated dynamics of hosts and parasitoids on the Åland patch geometry. Each dot corresponds to a single patch. Inset: the prevalence of the hosts (dashed line) and parasitoids (solid line) as a function of time. As spreading widths we have used  $w_h = 1000$  m,  $w_p = 500$  m. The annual death probability is  $\delta = 0.9$  and the host and parasitoid spreading rate parameters are  $\lambda_h = 100$  and  $\lambda_p = 1400$ . A fraction of 0.01 of the hosts spreads randomly to all patches. The archipelago is roughly  $60 \text{ km} \times 80 \text{ km}$  in size.

## 6. Discussion

The change between the patterned and non-patterned cases is rather abrupt in terms of several quantities. This leads naturally to the question whether the phenomenon is actually a phase transition. We argue that this is not the case due to several reasons. First, since phase transitions are defined only for infinite systems, the transition in plots such as Fig. 8 should become sharper as the system size increases. However the behavior remains essentially the same as in Fig. 8 for a wide range of system sizes, except for

the fact that for the smallest systems, the highest value the average domain wall length assumes becomes smaller due to finite-size effects. In any case, no sharpening of the transition is observed, and in this respect the correct description of the behavior is as a continuous crossover.

Second, similar models have been studied with the transition aspect in mind. The most relevant one for the present discussion is that by Wood and coworkers [52, 53], which deals with a symmetric three-state model of discrete coupled oscillators. It has been found that the system does not have a phase transition in two dimensions but does in three and higher dimensions. However, in two dimensions, there is a continuous change in the order parameter around the region of the parameter space where the transition would take place in higher dimensions. This is similar to what has been observed here for the average domain wall lengths, giving further credibility for the interpretation of the change from non-oscillatory to oscillatory behavior as a continuous cross-over.

The eigenvalue structure in the non-patterned case also speaks in favor of the absence of a sharp transition. We get a complex conjugate eigenvalue pair for the matrix  $a_{\sigma,\sigma'}$  in Eq. (14) even in the non-patterned case. The difference lies in the relative magnitudes of the oscillation and decay time scales. So, even if the ratio of the timescales were used instead of the average domain wall length, there would be no sharp transition (cf. Fig. 15). This can be viewed as a consequence of the corrected MF approach yielding a stable fixed point both in the patterned and the non-patterned regimes. As a conclusion, the difference between the two is strictly speaking only quantitative, or – put in other words – in the non-patterned case the spatial correlations are much more suppressed than in the patterned one. However, on the other hand, the quantitative difference between the cases is rather huge: There are practically no patterns in the non-oscillatory systems as can be seen by looking at the system itself (Fig. 1), the average domain wall length (Fig. 8), and the random walk experiments outlined in Section 2.3, for example. Therefore, discussing these two regimes as different appears justified.

In addition to the discrete-space discrete-time setting studied here, the methods of analysis and characterization of patterns and dynamics are equally applicable to systems with continuous time or space, for example that in Ref. [49]. Applying the methodology to such systems might reveal differences between them and their discrete-space counterparts. Studies of these would be interesting already as such. One possible cause of the differences is that the discretization of space into lattice cells often comes with implicit locally density-dependent establishment, i.e. the local population density is restricted such that only one individual can be present at one site at a time. Continuous-space approaches typically do not have such restrictions unless explicitly included.

A very similar system restricted to nearest-neighbour spreading has been recently studied [44, 46, 47] both analytically using the pair approximation and numerically. The authors of these articles have found that the co-existence phase is divided into two regions. These are oscillatory and non-oscillatory coexistence. The similarity to the present case is striking. It has been concluded in [44, 46, 47] from the pair approximation

that the oscillations are a limit cycle, and indirectly that, since there are oscillations also in the spatially extended counterpart, they have to be limit cycles as well. Comparing to the present results reveals that such conclusions cannot be made without further evidence; the possibility of noise-sustained oscillations remains, and for small systems even that of two kinds of oscillatory regimes. While further studies would be needed to resolve this issue, note that in some cases the amplitude fluctuates in a way that appears similar to the fluctuations in the present case. One example is given by Fig. 9a of Ref. [47]. On the other hand, there are established results on two-dimensional three-state dynamic lattice models with limit cycle oscillations [64]. Furthermore, processes on excitable media have been recently characterized in terms of prey–predator systems [65], and the machinery introduced here could provide tools for studying those as well.

Other comparable approaches taken recently include Refs. [66, 67]. In these works, a simplified model of two connected patches is studied, and the oscillations are made dependent either on the phase or the amplitude in the phase space. Both lead to stabilized oscillations. However, Eq. (14) explicitly forbids such dependencies in the present case, and therefore the mechanisms suggested in [66, 67] cannot be the root cause of the stability in the spatially extended case studied here.

Another interesting approach is to map related population models [24, 16] to the complex Ginzburg-Landau equation [29]. The mappings rely on the existence of an unstable fixed point [68], and the oscillations are classical limit cycles. Therefore, these studies and the present one can be described as complementary approaches to each other.

While the present model is without doubt castable as a partial differential equation at least in an approximative manner, it is an open question of what the outcome from such equations would be. Since the fully-mixed approximation can have both a stable and an unstable fixed point, a mapping to the CGLE along the lines of [16] would not work, and further complications are also caused by the highly asymmetric reaction rates [68]. Due to these reasons, it is not immediately clear that the picture of noise-sustained oscillations linked to patterns via spontaneous synchronizations would be captured by such a treatment. In any case, this kind of analysis offers an intriguing issue for future studies.

## 7. Conclusion

A model of two-species dynamics defined and treated in the language of hosts and parasitoids but equally applicable to prey–predator systems as well has been studied. In addition to extinct states, the system shows two kinds of coexistence, depending on the parameters. These are a patterned state with oscillating population densities and a non-patterned state with populations homogeneously distributed in space, and densities that fluctuate around their respective averages. This contribution contains two closely tied lines of work. One characterizes the patterns via coarse-graining the habitat space to domains in which a given species or empty space is dominant. The other concentrates

on the dynamics of the system.

The coarse-grained domains allow for a definition of domain walls as the lines separating the domains, and vortices as their corner points. From these, we compute several quantities, such as the instantaneous vortex velocities, their lifetime, the lengths of the domain walls, and ones describing the geometry of the domains in the vicinity of the vortices. Invariably, these quantities reveal the division of the parameter space into two kinds of coexistence. We have argued that these two regions are separated by a continuous cross-over rather than a conventional phase transition. We have also reasoned why the vortex number process is not comparable to that in the CGLE [29, 54, 55]. The main argument is based on the fact that the process is not memoryless.

The dynamics has been studied using Poincaré maps [56]. We have found out that as a stochastic dynamical system, the present one is two-dimensional. In other words, the dynamics is adequately described in terms of the two population densities and the unit-time advancing mapping, the Poincaré map, of the two. No further dynamical variables nor history-dependence are needed. In addition, for large systems the Poincaré maps are linear leading to an easy characterization of the behavior using eigenvalue analysis. In both the patterned and the non-patterned case, this reveals a stable fixed point with oscillatory transients. However, between the cases there is a huge difference in the level of separation between the associated oscillation and decay time scales. This also leads to a direct connection between the patterning and the dynamics, since the ratio of the two timescales has been shown to be closely related to the average domain wall lengths. The amplitude fluctuations have also been given a spatial interpretation as an irregular sequence of spontaneous synchronization and desynchronization events of coupled oscillators [58] whose role in this setting is played by mesoscopic subsystems.

We have also compared the average densities in the system to those predicted by a mean-field theory. We have introduced corrections to the MF equations on two levels based on series expansions and simulated data. In both zeroth- and first-order settings, the cross-over between the patterned and the non-patterned cases is visible and crucial.

The results have been compared to earlier literature. There are numerous results on related systems where oscillations have been recovered. In some of these, the oscillations might in fact be noise-sustained in character. Interesting candidates to study this possibility include [44, 46, 47, 50, 51]. In all of these, the machinery for pattern characterization introduced here could be applied to produce further insight.

We have applied the analysis briefly to the empirical metapopulation landscape of a butterfly and its parasitoids wasp [59, 60]. Future prospects include studying these issues further - we have merely highlighted the applicability of the results presented here. Studying such systems could, for instance, let one approach the question of how to tell the difference between patterns caused by inhomogeneities in the landscape and those that are spontaneously formed even on homogeneous substrates. Such extensions are naturally motivated also from the ecologists' point of view since metapopulation ecology often involves such landscapes [32].

*Acknowledgments*

Ilkka Hanski and Otso Ovaskainen (Univ. Helsinki, Metapopulation Research Group) are thanked for stimulating discussions and Lasse Laurson for assistance. This work was supported by the Academy of Finland through the Center of Excellence program (M.A. and M.P.) and Deutsche Forschungsgemeinschaft via SFB 611 (M.R.). The authors thank the Lorentz center (Leiden, Netherlands) for kind hospitality.

**References**

- [1] K.-i. Tainaka, Phys. Rev. E **50**, 3401 (1994).
- [2] R. Imbihl and G. Ertl, Chem. Rev. **95**, 697 (1995).
- [3] G. Szabó, A. Szolnoki, T. Antal, and I. Borsos, Phys. Rev. E **55**, 5275 (1997).
- [4] E. V. Albano, Phys. Rev. E **57**, 6840 (1998).
- [5] G. Szabó, M. A. Santos, and J. F. F. Mendes, Phys. Rev. E **60**, 3776 (1999).
- [6] V. P. Zhdanov, Phys. Rev. E **59**, 6292 (1999).
- [7] V. P. Zhdanov, Physica D **144**, 87 (2000).
- [8] G. A. Tsekouras and A. Provata, Phys. Rev. E **65**, 016204 (2002).
- [9] V. P. Zhdanov, Surf. Sci. Rep. **45**, 231 (2002).
- [10] G. Szabo and A. Szolnoki, Phys. Rev. E **65**, 036115 (2002).
- [11] T. Lele and J. Lauterbach, Chaos **12**, 164 (2002)
- [12] A. Provata and G. A. Tsekouras, Phys. Rev. E **67**, 056602 (2003).
- [13] A. Szolnoki and G. Szabó, Phys. Rev. E **70**, 027101 (2004).
- [14] A. Traulsen and J. C. Claussen, Phys. Rev. E **70**, 046128 (2004).
- [15] A. Szolnoki, G. Szabo, and M. Ravasz, Phys. Rev. E **71**, 027102 (2005).
- [16] T. Reichenbach, M. Mobilia, and E. Frey, J. Theor. Biol. **251**, 368 (2008).
- [17] R. V. Solé and J. Bascompte, *Self-Organization in Complex Ecosystems*, (Princeton University Press, Princeton, 2006).
- [18] W. S. C. Gurney, A. R. Veitch, I. Cruickshank, and G. McGeachin, Ecology **79**, 2516 (1998).
- [19] M. Pascual, M. Roy, F. Guichard, and G. Flierl, Phil. Trans. Roy. Soc. Lond. B **357**, 657 (2002).
- [20] F. Zhang, Z. Li, and C. Hui, Ecol. Modell. **193**, 721 (2006).
- [21] T. Nguyen-Huu, C. Lett, J. C. Poggiale, and P. Auger, Ecol. Modell. **197** 290 (2006).
- [22] M. Mobilia, I. T. Georgiev, and U. C. Täuber, J. Stat. Phys. **128**, 447 (2007).
- [23] C. Briggs and M. F. Hoopes, Theor. Pop. Biol. **65**, 299 (2004).
- [24] T. Reichenbach, M. Mobilia, and E. Frey, Nature **448**, 1046 (2007).
- [25] A. J. Lotka, J. Am. Chem. Soc. **42**, 1595 (1920).
- [26] D. E. Clapham, Cell **80**, 259 (1995).
- [27] M. J. Berridge, J. Physiol. **299**, 291 (1997).
- [28] M. Falcke, Adv. Phys. **53**, 255 (2004).
- [29] I. S. Aranson and L. Kramer, Rev. Mod. Phys. **74**, 99 (2002).
- [30] W. Murdoch, C. J. Briggs, and S. Swarbrick, Science **309**, 610 (2005).
- [31] D. J. Murrel, Am. Nat. **166**, 354 (2005).
- [32] I. Hanski, Nature **396**, 41 (1998).
- [33] X. Lambin, D. A. Elston, S. J. Petty, and J. L. MacKinnon, Proc. Roy. Soc. Lond. B **265**, 1491 (1998).
- [34] J. van de Koppel, M. Rietkerk, N. Dankers, and P. M. J. Herrman, Am. Nat. **165**, E66 (2005).
- [35] E. Ranta and V. Kaitala, Nature **390**, 456 (1997).
- [36] I. Hanski, H. Henttonen, E. Korpimäki, L. Oksanen, and P. Turchin, Ecology **82**, 1505 (2001).
- [37] J. van de Koppel, J. C. Gascoigne, G. Theraulaz, M. Rietkerk, W. M. Mooij, P. M. J. Herman, Science **322**, 739 (2008).

- [38] M. Peltomäki, M. Rost, and M. Alava, *Phys. Rev. E* **78**, 050903(R) (2008).
- [39] M.P. Hassell, H.N. Comins, and R.M. May, *Nature* **353**, 255 (1991).
- [40] R. Anderson and R. May, *Infectious Diseases of Human, Dynamics and Control*, (Oxford University Press, Oxford, 1995).
- [41] D. Jungnickel, *Graphs, Networks and Algorithms*, (Springer-Verlag, Berlin, 1999).
- [42] R. K. Ahuja, T. L. Magnanti, and J. B. Orlin, *Network flows: theory, algorithms, and applications*, (Prentice Hall, Eaglewood Cliffs, New Jersey, 1993).
- [43] D. ben-Avraham and J. Köhler, *Phys. Rev. A* **45**, 8358 (1992).
- [44] J. E. Satulovsky and T. Tomé, *Phys. Rev. E* **49**, 5073 (1994).
- [45] M. Peltomäki, V. Vuorinen, M. Alava, and M. Rost, *Phys. Rev. E* **72**, 046134 (2005).
- [46] T. Tomé and K.C. de Carvalho, *J. Phys. A Math. Gen.* **40**, 12901 (2007).
- [47] E. Arashiro, A. L. Rodrigues, M. J. de Oliveira, and T. Tomé, *Phys. Rev. E* **77**, 061909 (2008).
- [48] M. Pascual, P. Mazzega, and S. A. Levin, *Ecology* **82**, 2357 (2001).
- [49] O. Ovaskainen and S. Cornell, *Proc. Natl. Acad. Sci.* **103**, 12781 (2006).
- [50] T. Antal and M. Droz, *Phys. Rev. E* **63**, 056119 (2001).
- [51] T. Antal, M. Droz, A. Lipowski, and G. Ódor, *Phys. Rev. E* **64**, 036118 (2001).
- [52] K. Wood, C. Van den Broeck, R. Kawai, and K. Lindenberg, *Phys. Rev. Lett.* **96**, 145701 (2006).
- [53] K. Wood, C. van den Broeck, R. Kawai, and K. Lindenberg, *Phys. Rev. E* **74**, 031113 (2006).
- [54] L. Gil, J. Lega, and J. L. Meunier, *Phys. Rev. A* **41**, 1138 (1990).
- [55] H. Wang, *Phys. Rev. Lett.* **93**, 154101 (2004).
- [56] G. M. Zaslavsky, *Physics of Chaos in Hamiltonian Systems*, (Imperial College Press, London, 1998).
- [57] N.H. Packard, J.P. Crutchfield, J.D. Farmer, and R.S. Shaw, *Phys. Rev. Lett.* **45**, 712 (1980).
- [58] J. A. Acebrón, L. L. Bonilla, C. J. P. Vicente, F. Ritort, and R. Spigler, *Rev. Mod. Phys.* **77**, 137 (2005).
- [59] S. van Nouhuys and I. Hanski, *J. Anim. Ecol.* **71**, 639 (2002).
- [60] S. van Nouhyus and I. Hanski, in *On the Wings of Checkerspots: A Model system for Population Biology*, eds. P. R. Erlich and I. Hanski, (Oxford University Press, Oxford, 2004).
- [61] I. Hanski, *J. Anim. Ecol.* **63**, 151 (1994).
- [62] O. Ovaskainen and I. Hanski, *Theor. Pop. Biol.* **60**, 281 (2001).
- [63] V. Vuorinen, M. Peltomäki, M. Rost, and M. Alava, *Eur. Phys. J. B* **38**, 261 (2004).
- [64] G. A. Tsekouras and A. Provata, *Eur. Phys. J. B* **52**, 107 (2006).
- [65] N. F. Otani, A. Mo, S. Mannava, F. H. Fenton, E. M. Cherry, S. Luther, and R. F. Gilmour Jr., *Phys. Rev. E* **78**, 021913 (2008).
- [66] R. Abta, M. Schiffer, and N. M. Shnerb, *Phys. Rev. Lett.* **98**, 098104 (2007).
- [67] R. Abta and N. M. Shnerb, *Phys. Rev. E* **75**, 051914 (2007).
- [68] M. Peltomäki and M. Alava, *Phys. Rev. E* **78**, 031906 (2008).